Siddiqui, T., Stolle, C., Lühr, H. (2017): Longitude-dependent lunar tidal modulation of the equatorial electrojet during stratospheric sudden warmings. - *Journal of Geophysical Research*, *122*, 3, pp. 3760—3776.
DOI: http://doi.org/10.1002/2016JA023609

AGU PUBLICATIONS

JGR

Journal of Geophysical Research: Space Physics

RESEARCH ARTICLE
10.1002/2016JA023609

Key Points:
- Results show the difference in lunitidal enhancements in Peruvian and Indian sectors during major SSWs and a non-SSW winter
- Major longitudinal variability in lunitidal enhancement in EEJ in the Peruvian and Indian sectors during 2009 SSW event
- The lunar tidal amplitude derived from neutral measurements is similar in both the sectors and shows lesser longitudinal variability

Correspondence to:
T. A. Siddiqui,
tarique@gfz-potsdam.de

Citation:
Siddiqui, T. A., C. Stolle, and H. Lühr (2017), Longitude-dependent lunar tidal modulation of the equatorial electrojet during stratospheric sudden warmings, *J. Geophys. Res. Space Physics*, *122*, 3760–3776, doi:10.1002/2016JA023609.

Received 20 OCT 2016
Accepted 7 MAR 2017
Accepted article online 21 MAR 2017
Published online 25 MAR 2017

Longitude-dependent lunar tidal modulation of the equatorial electrojet during stratospheric sudden warmings

Tarique A. Siddiqui[1,2], Claudia Stolle[1,2], and Hermann Lühr[1]

[1]GFZ German Research Centre for Geosciences, Potsdam, Germany, [2]Institute of Earth and Environmental Science, University of Potsdam, Potsdam, Germany

Abstract The effects of coupling between different layers of the atmosphere during Stratospheric Sudden Warming (SSW) events have been studied quite extensively in the past few years, and in this context large lunitidal enhancements in the equatorial ionosphere have also been widely discussed. In this study we report about the longitudinal variabilities in lunitidal enhancement in the equatorial electrojet (EEJ) during SSWs through ground and space observations in the Peruvian and Indian sectors. We observe that the amplification of lunitidal oscillations in EEJ is significantly larger over the Peruvian sector in comparison to the Indian sector. We further compare the lunitidal oscillations in both the sectors during the 2005–2006 and 2008–2009 major SSW events and during a non-SSW winter of 2006–2007. It is found that the lunitidal amplitude in EEJ over the Peruvian sector showed similar enhancements during both the major SSWs, but the enhancements were notably different in the Indian sector. Independent from SSW events, we have also performed a climatological analysis of the lunar modulation of the EEJ during December solstice over both the sectors by using 10 years of CHAMP magnetic measurements and found larger lunitidal amplitudes over the Peruvian sector confirming the results from ground magnetometer observations. We have also analyzed the semidiurnal lunar tidal amplitude in neutral temperature measurements from Sounding of the Atmosphere using Broadband Emission Radiometry (SABER) at 110 km and found lesser longitudinal variability than the lunitidal amplitude in EEJ. Our results suggest that the longitudinal variabilities in lunitidal modulation of the EEJ during SSWs could be related to electrodynamics in the *E* region dynamo.

1. Introduction

Stratospheric Sudden Warmings (SSW) are large-scale meteorological events usually occurring in the winter hemisphere. The phenomenon of SSW was first observed by *Scherhag* [1952], and since then it has been studied extensively. SSWs are characterized by a weakening or sometimes even a reversal of the westerly winds in the northern stratosphere which leads to a sudden rise in polar stratospheric temperature by several tens of degrees [e.g., *Andrews et al.*, 1987]. The underlying mechanism behind SSWs is understood to be the nonlinear interaction of the vertically propagating planetary waves with the zonal mean flow as proposed by *Matsuno* [1971]. According to the World Meteorological Organization (WMO), SSWs can be classified into major and minor warming events based on the intensity of weakening of mean zonal wind at 60°N and 10 hPa. An SSW is classified as a major warming if the zonal wind at 60°N and 10 hPa shows a reversal from westerly to easterly. In case there is deceleration of the zonal wind but no reversal, then it is classified as a minor warming.

Although SSWs occur at polar stratospheric heights, their impact can be detected widely across higher altitudes. At high latitudes, observational and modeling studies suggest that SSWs result in cooling of the mesosphere [e.g., *Labitzke*, 1972; *Liu and Roble*, 2002; *Cho et al.*, 2004] and warming of the lower thermosphere [e.g., *Funke et al.*, 2010]. At middle latitudes, SSWs have been reported to be the cause behind alternating regions of warming and cooling in the ionosphere [*Goncharenko and Zhang*, 2008]. At low latitudes, SSW related perturbations in the ionosphere have also been seen in different parameters such as vertical plasma drifts [e.g., *Chau et al.*, 2009, 2010], the equatorial electrojet [e.g., *Yamazaki et al.*, 2012], and total electron content [*Goncharenko et al.*, 2010]. The longitudinal variabilities in the ionosphere during the 2009 major SSW in $E \times B$ drifts have also been observed through model simulations [e.g., *Fang et al.*, 2012]. Their results showed that the longitudinal variability of the neutral winds and the strength of the geomagnetic field could be the reason behind the longitudinal variation of vertical drifts. At equatorial and low-latitudinal regions of the ionosphere, one characteristic signature which has been observed during SSWs is a clear semidiurnal

perturbation pattern which shifts in time at later days. This shifting pattern was suggested by *Fejer et al.* [2010] to be due to the enhancement of semidiurnal lunar (M_2) tide during SSWs. They also observed these temporal perturbations in the equatorial electrojet in different longitudinal sectors. Usually, the perturbations were seen to occur at first in the American sector and lastly in the Pacific sector. The perturbations were also recorded to be strongest in the American sector. However, a quantitative comparison between the lunitidal enhancements in different longitudinal sectors during SSWs was not presented. Large lunitidal amplitudes in the equatorial electrojet (EEJ) during SSWs have also been reported from ground-based and satellite observations [e.g., *Park et al.*, 2012; *Yamazaki et al.*, 2012; *Yamazaki*, 2013; *Siddiqui et al.*, 2015a]. The readers may refer to a comprehensive review by *Chau et al.* [2012] for more details on impacts of SSW on the equatorial ionosphere.

The equatorial electrojet (EEJ) is a narrow band of an intense electric current confined to a latitude band of about $\pm 3°$ and flowing above the magnetic dip equator in the daytime *E* region of the ionosphere. Numerous studies have reported about the important characteristics of the EEJ based on the data from ground observatories and satellites [e.g., *Doumouya et al.*, 1998; *Rigoti et al.*, 1999; *Jadhav et al.*, 2002; *Lühr et al.*, 2004]. The EEJ current system is primarily driven by the dynamo action of tidal winds in the *E* region of the ionosphere. The atmospheric tides driven by solar heating constitute the dominant driver of this current system. In comparison, the effect of the gravitationally forced lunar tides is rather small. A comprehensive review on the EEJ can be found in *Forbes* [1981].

Lunitidal oscillations in horizontal component of magnetic field, *H*, at an equatorial station were first derived by *Bartels* [1936] at Huancayo, and the amplitudes were found to be significantly greater than at magnetic stations in higher latitudes. On certain days, the lunar influence in the EEJ was seen to become considerably large and even comparable to the solar effects. The existence of these "big L" days was first reported by *Bartels and Johnston* [1940] from ground-based magnetic observations at Huancayo in Peru. Subsequently, large lunitidal amplitudes were also computed at equatorial stations in Kodaikanal, India [*Rao and Sivaraman*, 1958] and Ibadan, Nigeria [*Onwumechilli and Alexander*, 1959]. The electrojet was attributed by *Forbush and Casaverde* [1961] as the reason for large lunitidal variation at Huancayo. *Rastogi* [1963] also reported that the lunitidal oscillations in *H* at stations close to the magnetic equator are greatly affected by the electrojet currents. Using a chain of magnetic observatories in Peru, he found that the semidiurnal lunar variations in daily range of *H* during December solstice at Huancayo (12.1°S, 75.2°W), which is located under the EEJ, were 4 times greater than at Talara (4.6°S, 81.3°W), which is located outside the EEJ. *Rastogi and Trivedi* [1970] also demonstrated the longitudinal variation of semidiurnal lunar tide (M_2) in EEJ. Using the horizontal magnetic intensity data at Huancayo (12.1°S, 75.2°W), Addis Ababa (9.0°N, 38.7°E), Trivandrum (8.5°N, 76.9°E), Koror (7.3°N, 134.5°E) and Jarvis (0.4°S, 160.0°W), they compared the amplitude of M_2 at all these stations and found the M_2 amplitude during December solstice at Huancayo to be 8.7 nT compared to 4 nT in Trivandrum. Further, their results also showed an increase in the M_2 amplitudes with an increase in the solar daily range of *H*. Hence, they concluded that the lunitidal oscillations in *H* show a strong longitudinal variability near the magnetic equator, and it is related to the longitudinal variations of EEJ. This variability was not only observed in the EEJ but also in the midday values of critical frequency (f_0F_2). The lunar semidiurnal variations in f_0F_2 also showed a maximum in the South American zone and a minimum over the Indian zone. *Rastogi* [1962a] suggested based on these observations that enhancement of the lunitidal variation over the dip equator in f_0F_2 is closely related to the equatorial electrojet. *Stening et al.* [2002] computed the amplitude and phases of lunitidal variations in *H* at many observatories in different latitudes and longitudes and determined the M_2 amplitude during December at Huancayo (Peru) and Trivandrum (India) to be 20.5 nT and 12.1 nT, respectively. They attributed the large lunitidal amplitude at Huancayo during December to higher Cowling conductivity over that region which results in the larger intensity of EEJ. However, *Rastogi* [1962b] has argued that the longitudinal variation of Cowling conductivity along the dip equator is too small to explain the difference in EEJ intensities and suggested a longitudinal variation in the tidal velocities to explain the larger lunitidal amplitude in EEJ over Peru as compared to over India.

This study follows the previous work by *Siddiqui et al.* [2015a, 2015b] in which they computed the lunitidal enhancements in EEJ at Huancayo during SSW and non-SSW winters and also showed a good correlation between the timing of lunitidal amplifications and the onset of stratospheric warmings. In this study we investigate the response of EEJ to SSW events in different longitudinal sectors. By quantitatively comparing the lunitidal enhancements in the Peruvian and Indian sectors using ground-based and satellite observations we suggest plausible causes for the observed longitudinal variabilities.

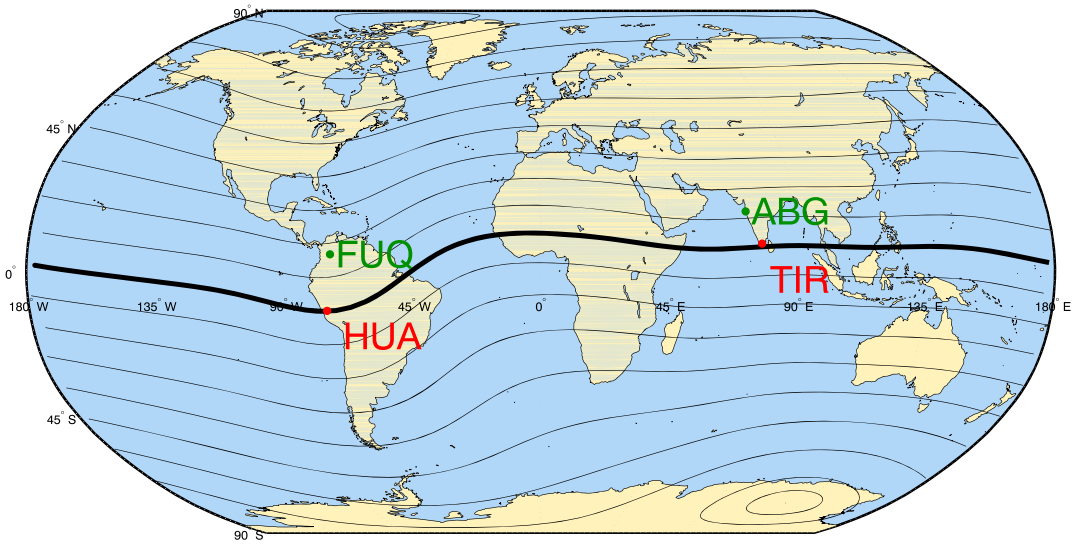

Figure 1. The locations of the observatories in the Peruvian and Indian sectors are presented in this plot. The black lines represent the quasi-dipole lines including the dip equator which is marked in bold black color. The equatorial observatories are marked with red dots, whereas the nonequatorial observatories are denoted with green dots.

We describe the various data sets used in this study in section 2. In section 3 we introduce our approach for determining the strength of the lunar tidal modulation of the EEJ and in the neutral temperature measurements. In section4 we present our observations followed by discussion in section 5. The conclusions from this work are presented in the final section.

2. Data Set

In this study we use multiple data sets to investigate the longitudinal variabilities of the lunitidal oscillations during SSWs. The details regarding the various sources of data considered in this study are elucidated in the following paragraphs.

To study the longitudinal characteristics of lunar tides in the EEJ, horizontal (*H*) component recordings from ground-based magnetometers in the Indian and Peruvian sectors have been utilized. Hourly means of the geomagnetic *H* component at Huancayo, HUA, (−12.05°N, 284.67°E, 0.59° dip latitude), Fuquene, FUQ, (18.11°N, 293.85°E, 17.06° dip latitude), Tirunelveli, TIR, (8.7°N, 77.8°E, 0.59° dip latitude), and Alibag, ABG, (18.6°N, 72.9°E, 13.67° dip latitude) for the following periods were downloaded from the website of World Data Centre for Geomagnetism, Edinburgh: (a) December 2005 to February 2006 , (b) December 2006 to February 2007, and (c) December 2008 to February 2009.

Figure 1 shows the location of the observatories used in this study. The black lines represent the quasi-dipole lines including the dip equator which is plotted in bold black color. The locations of equatorial observatories are marked with red dots, while the location of nonequatorial observatories are represented with green dots.

The pair of magnetometers in both the sectors have been chosen such that one of the observatories is situated directly beneath the equatorial electrojet (HUA & TIR) and the other observatories (FUQ & ABG) lie outside the influence of EEJ. The purpose of using this approach is that a major part of solar quiet (S_q) daily magnetic variation at an equatorial observatory can be removed by using the S_q variation at a nonequatorial observatory [e.g., *Manoj et al.*, 2006]. The enhancement of lunitidal amplitudes in the EEJ has been compared in *Siddiqui et al.* [2015b] for both the cases when an equatorial station makes use of a reference station and when it is used alone. The lunitidal enhancements seemed better correlated with stratospheric observations of SSW when a suitable reference station was considered. Here Fuquene and Alibag serve as reference stations to the equatorial observatories at Huancayo and Tirunelveli, respectively.

For the purpose of direct comparison between ground and satellite observations, EEJ intensities derived from the CHAMP satellite measurements are also used in this study. The CHAMP satellite was launched into a circular, near-polar (inclination: 87.2°) orbit at 456 km altitude on 15 July 2000, and it provided highly precise

gravity and magnetic field measurements over a 10 year period. It circled the Earth about 15.5 times per day and its orbital plane precessed through local time at a rate of 1 h per 11 days. It required 131 days to cover all local times, considering both ascending and descending orbital nodes. The electrojet current strength was deduced from magnetic field measurements on board CHAMP. The readers may refer to *Lühr et al.* [2004] for a more detailed description of the EEJ determination from CHAMP measurements.

The V2.0 temperature measurements from the Sounding of the Atmosphere using Broadband Emission Radiometry (SABER) instrument on the Thermosphere Ionosphere Mesosphere Energetics and Dynamics (TIMED) satellite are used to estimate lunar tidal amplitude in neutral temperature at an altitude of 110 km.

To consider the dependence of the EEJ strength on solar activity, we apply the solar flux values $F_{10.7}$ in solar flux unit (sfu; 10^{-22} W m^{-2} Hz^{-1}) which are available at the GSFC/SPDF OMNIWeb interface at http://omniweb.gsfc.nasa.gov. The weakening of the northern polar vortex is quantitatively deduced from the zonal mean zonal wind (U) at 70°N and at 48 km altitude and from the temperature (T) at the North Pole and at 40 km altitude which were obtained from MERRA (Modern-Era Retrospective Analysis for Research and Application) maps (ftp://goldsmr3.sci.gsfc.nasa.gov/data/s4pa/MERRA/).

3. Methods of Analysis

3.1. Estimating Lunar Tidal Amplitude in EEJ From Ground Magnetic Records

Regular daily variations with period and subperiods of a solar day are found in ground magnetic records and are termed as geomagnetic solar (S) daily variations. Besides S there are also smaller periodic variations depending on lunar time called the geomagnetic lunar (L) daily variations. The amplitude of L is an order of magnitude smaller than S, and its dominant component is the semidiurnal variation (12.42 h) which displays a semimonthly variation (14.77 days) at a fixed local time. Normally, lunar modulation of the EEJ roughly amounts to about 15% of its intensity [e.g., *Onwumechilli*, 1963; *Lühr et al.*, 2012], but during certain "big L days" between November and February, lunar effects in the EEJ suddenly show an increase by 4–5 times [*Bartels and Johnston*, 1940]. One of the causes for these large lunitidal enhancements in the EEJ could be due to modified tidal propagation conditions during SSWs [*Forbes and Zhang*, 2012]. In this study we first investigate the lunar modulation of EEJ during SSWs in the Peruvian and Indian longitudinal sectors by using the ground-based magnetic recordings in these regions.

We employ the method as explained in *Siddiqui et al.* [2015b] to deduce the semimonthly lunar tidal amplitude from the H component of ground-based magnetic field recordings. Briefly, the electrojet strength is estimated by choosing a pair of stations such that one of the stations lies within the electrojet footprint, and the other is located outside of it, thus acting as a reference station to the former. The nighttime values are used as a reasonable approximation for removing the effects of the Earth's core and crustal field. The nighttime values, H_{MF}, are first subtracted individually from the horizontal component recordings, H, of both the equatorial and the reference station. Here H_{MF} represents the contributions of Earth's main field (MF) in the H component of ground-based magnetic field recordings.

$$\Delta H = H - H_{MF} \tag{1}$$

ΔH here reflects the daily variation with respect to the local midnight values. The electrojet strength, H_{EEJ}, is then estimated by computing the difference between the daily variations at the equatorial and the reference station.

$$H_{EEJ} = \Delta H_{EEJ} - \Delta H_{NonEEJ} \tag{2}$$

As mentioned in the earlier paragraphs, the stations chosen for the Peruvian sector are Huancayo and Fuquene, and in case of the Indian sector the stations are Tirunelveli and Alibag. For both these station pairs, the EEJ derived strength is then normalized to a solar flux level of 150 sfu and the data are then arranged into bins of 1 day by 1 h in local time (LT) from 08:00 to 16:00 h for an interval of 59 days. The dominant solar tidal variations are removed by subtracting the means over a 59 day period (two lunar months) for each local time hour. The amplitude of the semimonthly lunar wave (14.77 days) is then obtained by fast Fourier transform (FFT) for each local time hour. The amplitude thus obtained is then normalized for the expected diurnal variation of the ionospheric conductivity, C, following *Lühr et al.* [2008].

$$C = C_0 \sqrt{\cos\left\{\frac{\pi}{12\,h}(\mathrm{LT} - t_0)\right\}} \tag{3}$$

where $C_0 = 1$ indicates the peak conductivity and $t_0 = 12{:}30$ LT is the local time of the peak conductivity.

The semimonthly lunar wave over 59 days is estimated from the mean of normalized amplitudes for each local time bin. A sliding window of 59 days length advanced by 1 day is applied to estimate the day by day lunitidal amplitude.

3.2. Estimating Lunar Tidal Amplitude From the CHAMP Magnetometer Measurements

We further investigate the lunar modulation of EEJ during SSWs in the Peruvian and Indian longitudinal sectors by using the CHAMP magnetometer measurements. Since we are investigating the longitudinal variabilities in the lunar tide of the EEJ, we first sort the EEJ values derived from CHAMP, according to two longitudinal intervals each of 90° width around the Peruvian and Indian sectors. The Peruvian sector is represented by the longitudes between 235° and 325°E, while the longitudinal intervals between 45° and 135°E have been selected for the Indian sector. The EEJ dependence on solar activity is accounted by normalization using the statistical formula used by *Park et al.* [2012] (see equation (1))

$$\mathrm{EEJ}' = \frac{\mathrm{EEJ}}{\sqrt{\left(\frac{F_{10.7P}}{150} \times \left|\cos\frac{\pi}{12}(\mathrm{LT} - 12\,\mathrm{h})\right|\right)}} \tag{4}$$

where EEJ and EEJ′ are the original and normalized EEJ peak current densities [*Alken and Maus*, 2007], respectively and $F_{10.7P} = \frac{F_{10.7}+F_{10.7A}}{2}$ where $F_{10.7}$ is the observed value of solar radio emission at 10.7 cm for each day and $F_{10.7A}$ is the 81 day averaged value of $F_{10.7}$ index.

Further, following *Park et al.* [2012], a similar approach for estimating the semidiurnal lunar (M_2) tidal amplitude from the CHAMP EEJ data is applied in both these sectors. Instead of calculating zonally averaged EEJ′, which was used by them, we compute $\widetilde{\mathrm{EEJ}'}$ which is averaged over each longitudinal sector. The averaged values are then detrended by using a 39 day 1-D median filter. Since the M_2 tide appears Doppler shifted at a period of approximately 13 days in the moving frame of the CHAMP satellite [see *Park et al.*, 2012], three cycles of the 13 day oscillation corresponds to the filter length of 39 days. The M_2 amplitude is then evaluated for a moving window of 39 days length using the FFT. The window is moved forward by 1 day, and the same analysis is applied to subsequent days.

3.3. Estimating Lunar Tidal Amplitude From the SABER Temperature Measurements

The SABER neutral temperature measurements within ±5° latitude around Huancayo and Tirunelveli and at 110 km altitude are also analyzed to study the longitudinal variability of the M_2 during SSWs. The longitudinal interval corresponding to the Peruvian and Indian sectors have been considered as above, and the data are sorted for each day. For the estimation of M_2, we employ the method used by *Forbes and Zhang* [2012]. The Doppler-shifted M_2 lunar tide in the frame of SABER instrument on board the TIMED satellite corresponds to 11.85 days [*Forbes and Zhang*, 2012]. Using this fact, we start the procedure for the lunar tidal analysis by calculating residuals for each day by using a 12 day running mean background temperature centered on that day. The residuals are then fitted within a 12 day moving window using the least squares method to extract the semidiurnal lunar signal. The window is subsequently moved forward by 1 day at a time to determine the evolution of the M_2 tide during SSWs.

In the above analyses, although we have used different window sizes based on the M_2 and semimonthly lunar periods on the ground and on the two satellite frames, we do not expect a difference due to varying window lengths when comparing the lunitidal enhancements.

3.4. Identification of Sudden Stratospheric Warming Events Using the Concept of Polar Vortex Weakening

The concept of using polar vortex weakening (PVW) for characterizing the strength of SSW events was introduced by *Zhang and Forbes* [2014]. They used the daily time series of the zonal mean zonal wind (U) at 70°N and 48 km altitude and temperature (T) at North Pole and 40 km altitude from the MERRA reanalysis data set to describe the PVW. This same definition was then also used by *Chau et al.* [2015] and later by *Siddiqui et al.* [2015b] to demonstrate a correlation between the PVW characteristics and lunitidal enhancements in the upper mesosphere and in the EEJ, respectively.

In this study we also use the same definition of PVW to compare its timing with the lunitidal enhancements in the EEJ and in the SABER temperature measurements.

4. Observations and Results

4.1. Lunar Tidal Modulation of the EEJ During SSW

Figures 2–4 (top) present the diurnal magnetic field variations underneath the EEJ at the Huancayo and Tirunelveli observatories during December 2005 to February 2006, December 2008 to February 2009, and December 2006 to February 2007, respectively. Figures 2 and 3 include the SSW events of 2006 and 2009, while no SSW event (according to the WMO definition) was recorded during December 2006 to February 2007. Figures 2–4 (bottom) present the daily time series of the zonal mean zonal wind, U, (red curve) at 70°N and 48 km altitude and the temperature, T, (black curve) at North Pole and 40 km altitude for the above mentioned periods. The dashed black vertical lines in Figures 2 and 3 mark the days of peak PVW. The dashed blue vertical lines in Figure 2 denote multiple warming events that occurred prior to the intense event (denoted by dashed black line).

The development of major SSW events in 2006 can be seen in Figure 2. During this period multiple episodes of major warming events are recorded. The zonal mean wind at 70°N and at an altitude of 48 km starts to decelerate around 31st December, reverses its direction and reaches a minimum on 3rd January. The temperature starts to increase along with deceleration of the winds and peaks on the same day when the minimum in winds are recorded. Later episodes of warming reached their peaks on 11th, 18th and 22nd January. The fourth warming event is the most prolonged during this period with the zonal winds reversing and reaching almost 80 m/s in the westward direction.

The second episode of warming is larger than the first one and starts around 11th January. During this period, the equatorial electrojet first weakens for a couple of days and then develops a semidiurnal perturbation pattern with morning enhancement and afternoon weakening which shifts to later local times. The perturbation pattern is similar to the one described by *Fejer et al.* [2010] in case of the 2003 SSW event. A second perturbation pattern in EEJ starting around 28th January can also be seen in both these panels. As it has been reported earlier by *Fejer et al.* [2010], these perturbations are also seen first in the Peruvian sector and a few days later in the Indian sector. Another notable feature is the stronger perturbation patterns over the Peruvian sector than the Indian sector.

During the 2008–2009 winter, multiple warming events are not witnessed and can be seen in Figure 3. The zonal wind starts to decelerate around 18th January and reaches its minimum on 23rd while the temperature at the North Pole is also seen to peak during this period. The 2009 SSW event is one of the strongest and most prolonged SSW ever recorded in history [*Manney et al.*, 2009]. As seen earlier during the 2006 SSW event, in this case too, the EEJ intensity decreases at first and then after the peak warming around 26th January develops a similar semidiurnal pattern with morning enhancements and afternoon weakening which shifts to later times at both longitudes. It can be further seen that the semidiurnal pattern is much clearer and stronger in the Peruvian sector than in the Indian sector during this event.

Figure 4 presents the same plot as Figures 2 and 3 but during December 2006 to February 2007. According to WMO's definition of stratospheric warming, no SSW events are recorded during this period, however, we detect a minor episode of warming around 31 December. The temperature at the North Pole shows an enhancement, and the zonal wind also shows a deceleration, but it does not get reversed. A slightly weaker semidiurnal pattern compared to the one in Figure 2 can be seen around 2 January in the first two panels. The perturbation is much weaker as compared to major SSW events in Figures 2 and 3 in both sectors. The difference in the perturbations of EEJ intensity during stronger and weaker zonal wind reversal conditions is evident in these three plots. The observed perturbations can be attributed to the amplification of lunitidal oscillations in the equatorial electrojet during SSWs [*Fejer et al.*, 2010].

4.2. Lunar Tidal Amplitudes in EEJ and Neutral Temperature Measurements

The three panels in Figures 5–7 present the lunar tidal amplitudes that have been computed from the magnetometer recordings, peak EEJ intensity measurements from CHAMP, and SABER temperature data, respectively, during the SSW winters of 2006 and 2009 and during the non-SSW winter of 2007. The dashed black vertical lines denote the day of strongest PVW in Figures 5 and 6 in all the three panels. The solid black and red lines in these figures denote the lunitidal amplitudes in the Peruvian and Indian sectors, respectively.

4.2.1. 2006 SSW Event

Figure 5 (top) presents the semimonthly lunar tidal amplitude derived from H_{EEJ} which is clearly larger at Huancayo (Peru) than at Tirunelveli (India) during the 2006 SSW winter. A strong enhancement in both sectors starts toward the end of December followed by a peak in amplitude during the third week of January.

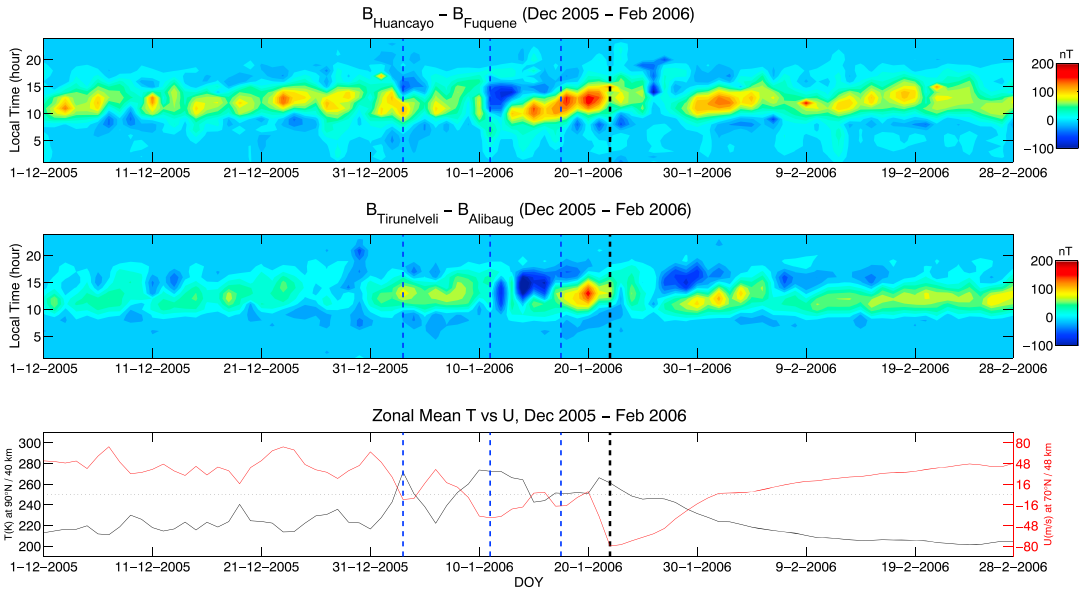

Figure 2. (top and middle) The daily variation of the EEJ at Huancayo, Peru and Tirunelveli, India, during December 2005 to February 2006. (bottom) The daily time series of the mean zonal wind (U) at 70°N and 48 km altitude (red curve) and temperature (T) at North Pole and 40 km (black curve) during the same period. The dashed black vertical line in each panel marks the peak polar vortex weakening (PVW) day. The dashed blue vertical lines denote the multiple episodes of warming prior to PVW during this time interval.

The peak PVW also takes place during this time, and the close correlation between these two phenomena was demonstrated in *Siddiqui et al.* [2015b]. In the Peruvian sector, the peak amplitude reaches a value of 42.2 nT and it occurs on 22 January, whereas in the Indian sector peak amplitude of 27.3 nT is achieved a day later on 23 January. The ratio between peak amplitudes at Huancayo and Tirunelveli is 1.5. As the days of peak PVW are quite similar for both the 2006 and 2009 SSW, the percentage changes between the prewarming and peak amplitudes are calculated relative to 1 January in both these cases. The relative changes in semimonthly lunar tidal amplitude for both the Peruvian and Indian longitudes are similar, being 131% and 126%, respectively.

In Figure 5 (middle), the M_2 amplitude from CHAMP peak EEJ intensity data is presented. The local time coverage of the CHAMP satellite during the 2006 SSW event was favorable in the sense that CHAMP recorded

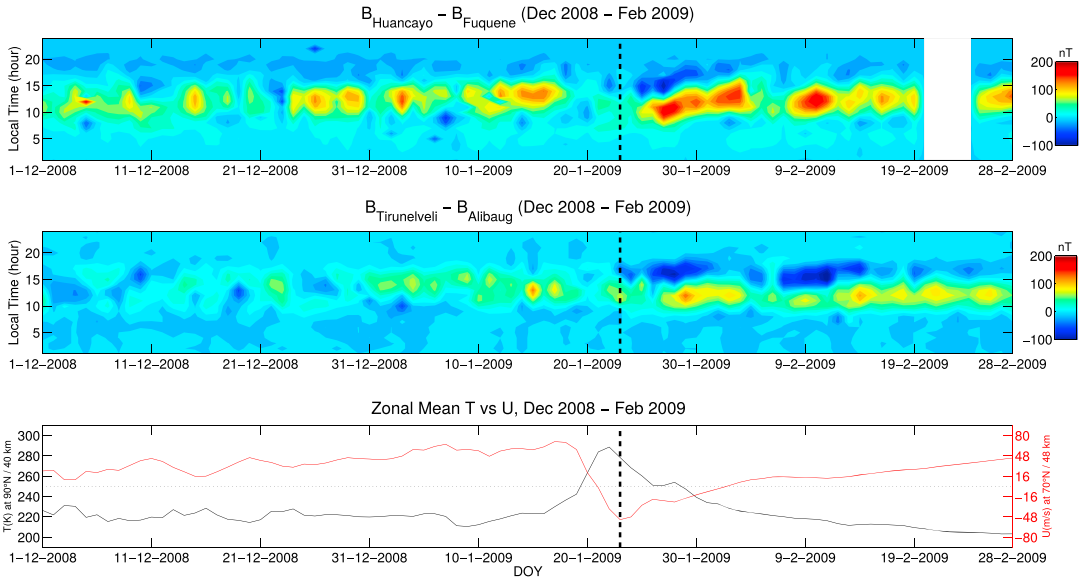

Figure 3. Same as Figure 2 but during the period December 2008 to February 2009.

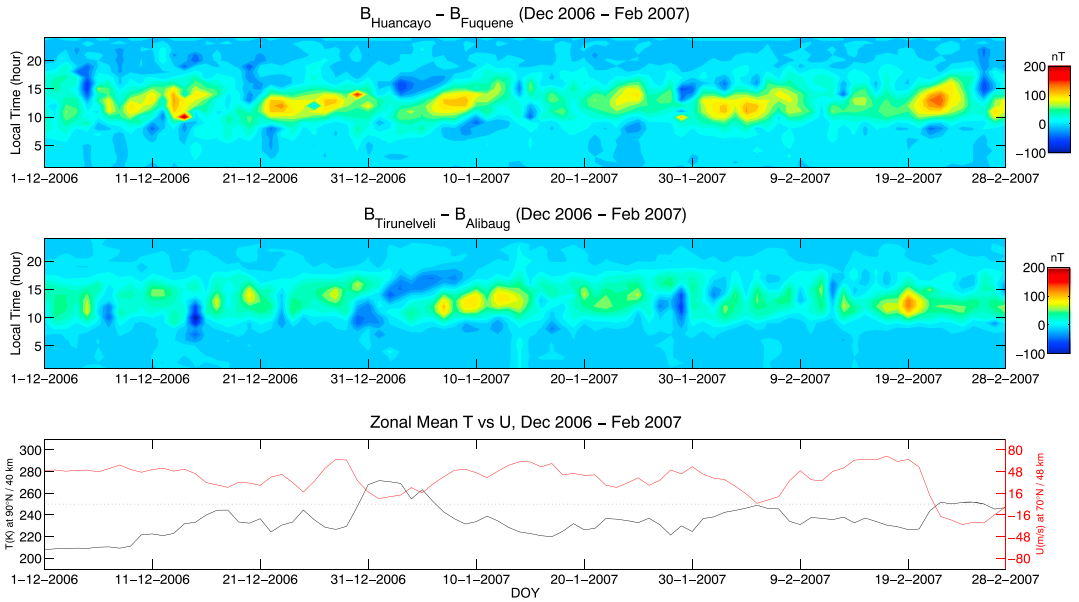

Figure 4. Same as Figure 2 but during the period December 2006 to February 2007.

the EEJ intensity during the daytime between 7 and 17 LT during December 2005 and January 2006. The enhancement in M_2 starts similarly toward the end of December as in the case of ground observations, and then the maximum M_2 amplitude is recorded during the third week of January around the time of peak PVW in both sectors. Here the lunitidal enhancement in the Peruvian sector is larger than in the Indian sector. The peak amplitudes, however, are recorded earlier than the day of PVW, and this is due to decreasing LT in the satellite frame. The local time was 12 LT on 31 December 2005 and moved to 10 LT on the day of observed PVW maximum. The M_2 amplitudes on the day of peak PVW are 74.4 (mA/m) and 48.3 (mA/m) for the Peruvian and Indian sectors, respectively, with the ratio again being 1.5. However, due to the varying LT in the satellite frame, the relative percentage changes are difficult to compare and therefore are not shown. In both the ground-based and space measurements the lunitidal enhancements start at similar time, and the level

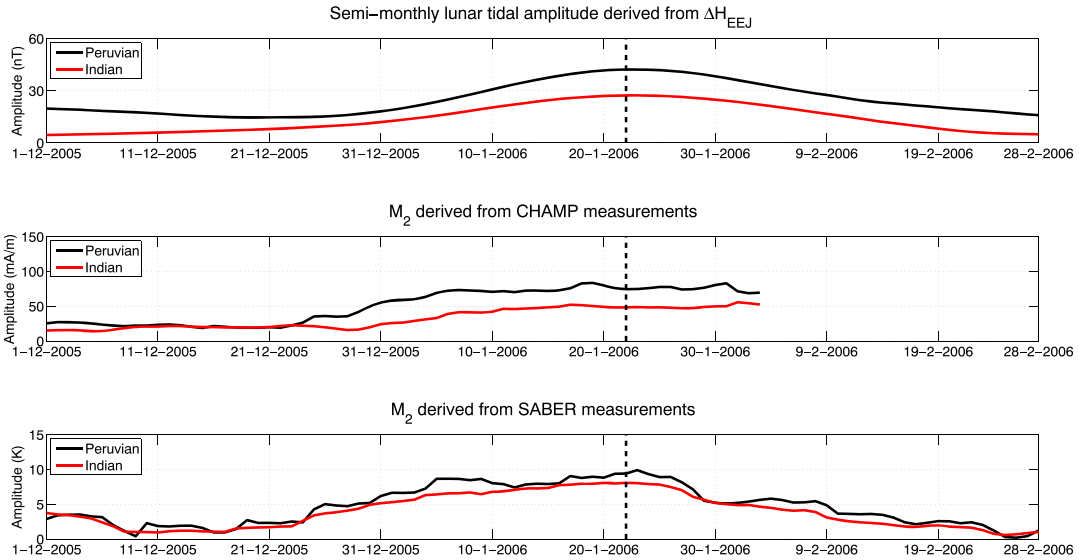

Figure 5. (top) The semimonthly lunar tidal amplitude in the EEJ derived from ground magnetometer recordings between December 2005 and February 2006. The black line denotes the lunitidal amplitude in the Peruvian sector, and the red line denotes the same in the Indian sector. (middle) The M_2 amplitude derived from CHAMP data during the same period and for the above two sectors. (bottom) The M_2 amplitude derived from SABER temperature measurements. The black vertical dashed line in all the panels denote the day of peak PVW.

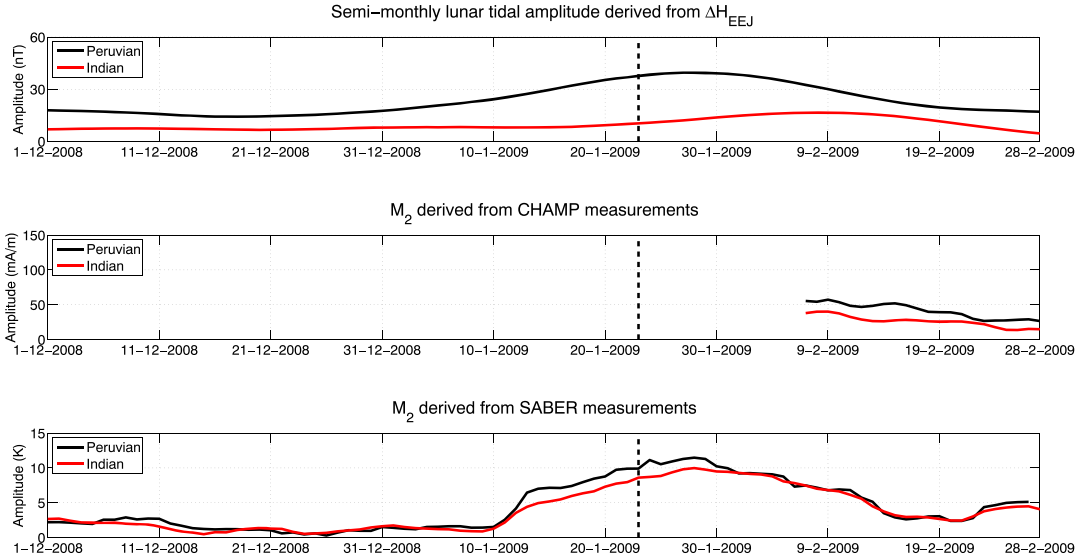

Figure 6. Same as in Figure 5 but only for the period December 2008 to February 2009.

of enhancements is also similar in both sectors. Overall, the semimonthly lunar tidal amplitude derived from magnetometer recordings and the M_2 amplitude derived from CHAMP satellite measurements show a good agreement with each other.

In Figure 5 (bottom) the M_2 amplitude derived from SABER temperature measurements is shown for both the sectors. The M_2 amplitude starts increasing during the last week of December and it reaches the peak value of 9.4 K (Peruvian sector) and 8.1 K (Indian sector) on 23 and 22 January, respectively, with the ratio between peak M_2 enhancements being 1.1. Thereafter, it shows a gradual decrease till the end of February in both the sectors. The M_2 enhancements in neutral temperature are similar in both the sectors, unlike the lunitidal enhancements in EEJ. The day of peak M_2 amplification in neutral temperature measurements compares quite well with the respective lunitidal peaks in EEJ derived from ground observations. The peak lunitidal amplitudes from ground magnetometer, CHAMP, and SABER measurements are presented in Table 1 along with their respective delays in timing relative to the PVW.

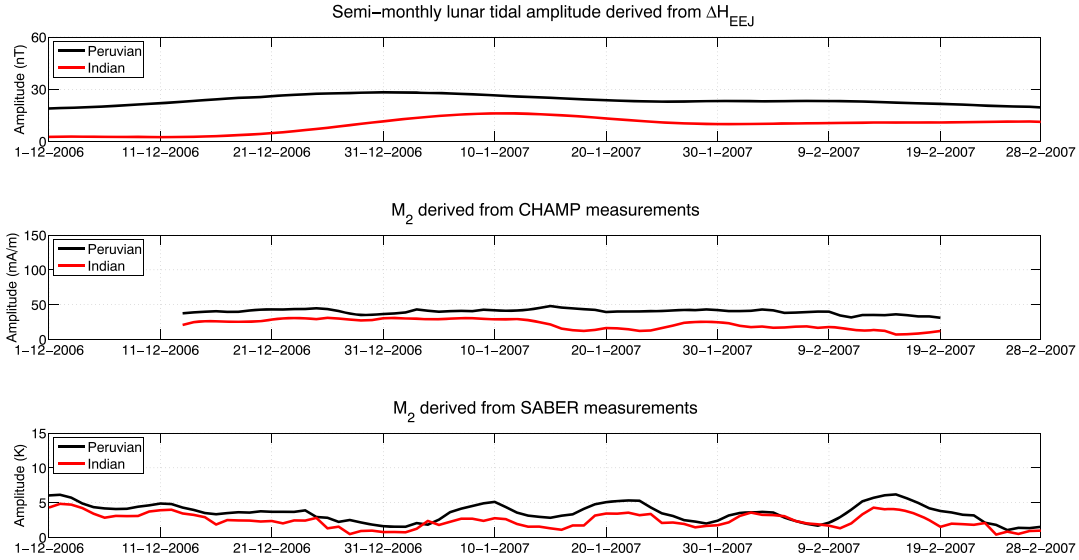

Figure 7. Same as in Figure 5 but only for the period December 2006 to February 2007.

Table 1. The Peak Semimonthly Lunitidal Amplitude From Ground Magnetometer Recordings, M_2 Amplitudes (on the Day of PVW) From CHAMP Data, and Peak M_2 Amplitudes From SABER Measurements in Both the Indian and Peruvian Sectors Are Presented Here[a]

Year	Date of PVWs	Sector	Ground Magnetometer (nT)	CHAMP (mA/m)	SABER (K)
2006	22 Jan	Peruvian	42.2 (0 day)	74.4	9.4 (1 day)
		Indian	27.3 (1 day)	48.3	8.1 (0 day)
2007		Peruvian	28.3	47.3	6.1
		Indian	16.0	28.9	4.8
2009	23 Jan	Peruvian	39.4 (4 days)		11.4 (5 days)
		Indian	16.5 (16 days)		9.9 (5 days)

[a]The values are followed by their respective delays in timing (wherever applicable) with respect to the PVW day.

4.2.2. 2009 SSW Event

Figure 6 (top) shows the semimonthly lunar tidal amplitude computed from ground magnetometer recordings during the 2008–2009 SSW winter. The lunitidal amplitude in EEJ at Huancayo shows a similar enhancement as in the case of 2005–2006 SSW event and reaches its peak 4 days after the day of PVW, whereas the enhancement at Tirunelveli is much smaller and its peak appears 16 days later than the PVW day. The peak amplitude at Huancayo during this event is 39.4 nT, and it is 16.5 nT at Tirunelveli with their ratio being equal to 2.4. The relative changes in lunitidal amplitude for both the Peruvian and Indian longitudes are 125% and 108%, respectively.

The peak lunitidal amplitude at Tirunelveli is attained during the postwarming phase when the wind direction started to change again from easterly to westerly and the temperature values started to reach pre-SSW levels. The 2006 and 2009 SSWs are both major warming events, and the lunar tidal enhancement at Huancayo is similar during both these major SSWs, as peak values are alike and the timing of enhancements closely follows the PVW. However, the timing and amplitude in the Indian sector are different during both these SSWs. The shifting semidiurnal perturbation in Figure 3 is clearly stronger in the Peruvian sector, while in the Indian sector the perturbation more resembles a solar diurnal variation, which suggests a weaker lunar influence on the EEJ.

In Figure 6 (middle), the M_2 amplitude computed from CHAMP peak EEJ intensity data is presented. However, during December 2008 to January 2009, CHAMP crossed the magnetic equator during nighttime hours (LT) and the local daytime coverage of EEJ resumed only during the first week of February 2009. The lunitidal amplitude can therefore be estimated only during February to March 2009 for this SSW winter, and a direct comparison between the top two panels is not possible likewise as in Figure 5. CHAMP precessed through 17 LT on 19 January 2009 and then moved to 16 LT on the day of observed PVW maximum. Here the M_2 amplitude in February is probably in the declining phase after a plausible enhancement during the SSW event. The amplitude is again consistently larger in the Peruvian sector than in the Indian sector.

Figure 6 (bottom) presents the M_2 amplitude in SABER temperature data. In both the sectors, the enhancement in M_2 begins after 10 January and the peak amplitude is achieved on 28 January with values of 10 K and 9.7 K in the Peruvian and Indian sectors, respectively, with the ratio of peaks being 1.03. The timing of peak PVW is recorded on 23 January for this SSW event. Post-SSW, the wind, and temperature values start to reach their pre-SSW levels, and the enhancement in M_2 amplitude also gradually subsides. The lunitidal amplification levels from SABER measurements are again similar in both the sectors and closely follow the semimonthly lunitidal amplification at Huancayo.

4.2.3. The 2006–2007 Northern Winter

In Figure 7, the lunitidal amplitudes from the three data sets are compared during the winter of 2006–2007 in which no major warming was recorded. In Figure 7 (top), unlike in the previous two figures, no sharp increase in the semimonthly lunar tidal amplitude is observed. Although a gentler enhancement can be seen toward the end of December in the Peruvian sector and in the first 10 days of January in the Indian sector, which could be either related to the seasonal enhancement of the lunar tide which happens during December solstice or to the moderate enhancement of stratospheric temperatures around 31 December. Also, the amplitude in the Peruvian sector is larger than in the Indian sector, as seen in the earlier two cases. The peak lunitidal amplitude at Huancayo is 28.3 nT on 31 December 2006 and 16 nT at Tirunelveli on 12 January and their ratio being equal to 1.7.

In Figure 7 (middle and bottom), the M_2 amplitude from CHAMP and SABER measurements does not show a clear enhancement in both the sectors as during the SSW winters. The CHAMP satellite precessed from 15 to 7 LT during this period, making it suitable to derive M_2 amplitude for this interval. Although the M_2 amplitudes remain less than 50 (mA/m) during the entire period in both the sectors, larger values are again observed over the Peruvian sector in this case. The M_2 amplitudes in the neutral temperature show no major enhancements during this winter, and the values remain less than 5 K over both the sectors during the entire time interval. A major difference in M_2 amplitudes is thus clearly visible between SSW and non-SSW winter periods. However, the M_2 amplitudes in neutral temperature measurements are similar over both the Peruvian and Indian sectors in all the three considered time intervals.

4.3. Phase Propagation of the Semimonthly Lunar Tide in EEJ

The lunar tide is an astronomical phenomenon, and therefore, its phase in general can be precisely determined. For example, *Lühr et al.* [2012] used 5 years of CHAMP data to investigate the phase propagation of the semimonthly lunar tide as a function of moon phase. They obtained a linear pattern of phase propagation with aging moon that is consistent with astronomical predictions [see *Lühr et al.*, 2012, Figure 3]. When fitting a regression line to the phase values of analyzed lunitidal waves that were determined independently for each local time hour, they obtained the following formula for the linear fit which estimates the local time (LT) of the maximum of the semimonthly wave for all moon phases.

$$\mathrm{LT} = 1.2(\mathrm{MP} - 12\,\mathrm{h}) + 8.5\,\mathrm{h} \tag{5}$$

The above equation, when written in terms of days from the new moon instead of moon phase, comes out to be [see *Siddiqui et al.*, 2015a, equation (6)]:

$$\mathrm{LT} = 0.98(d - d_0) + 8.5\,\mathrm{h} \tag{6}$$

where d is the number of days since new moon, LT, is the local time, and d_0 is on conversion from moon phase to days approximately equals 14.77 ($\approx \frac{12}{24} \times 29.53$) days.

As mentioned earlier the moon phase of 24 h is approximately equivalent to 29.53 days, whereas in our analysis we have used a window of $29.53 \times 2 \approx 59$ days. We tested the phase propagation of the semimonthly lunar tide during the three periods of analysis to verify if the wave periods extracted through the method described in section 3.1 can be attributed to lunar effects. In the following three subsections the phase propagation of the semimonthly lunar tide in the EEJ at Huancayo and Tirunelveli has been determined from the H component of ground-based magnetic field recordings during the periods covering the SSW events of 2006 and 2009 and the 2006–2007 non SSW winter, respectively.

4.3.1. 2006 SSW Event

In Figure 8 the phase propagation of the semimonthly lunar tide at the Peruvian and Indian sectors for a 59 day window starting from the day of a new moon during the 2005–2006 SSW event is presented. Here we have selected the window such that it starts and ends on the days of new moon and also covers the SSW period. The black dots and the red asterisks mark the phase propagation in the Peruvian and Indian sectors, respectively. The blue line is obtained by a linear regression fit made for the semimonthly propagating phase in the Peruvian sector (black dots) and is similar to the one mentioned in [*Lühr et al.*, 2012] (see their Figure 3). In cases of modified tidal propagation conditions such as during SSWs, the semimonthly lunar phase could show slight changes but here despite the enhanced wave activity during the SSW period, the phase of the semimonthly lunar tide resembles the expected pattern of phase propagation derived in *Lühr et al.* [2012] at both the Peruvian and Indian sectors. The phase propagation of the semimonthly lunar tide has been determined during the period when the SSW effects are strongest, and here it is likely that the applied method robustly filters out the effects of other tides and waves which can impact the results.

Further, the equation of the regression line obtained by least squares fitting is

$$\mathrm{LT} = 0.94(d - d_0) + 8.9\,\mathrm{h} \tag{7}$$

The regression parameters are also similar to the ones in equation (6), which supports the fact that the amplitudes are largely related to lunar effects.

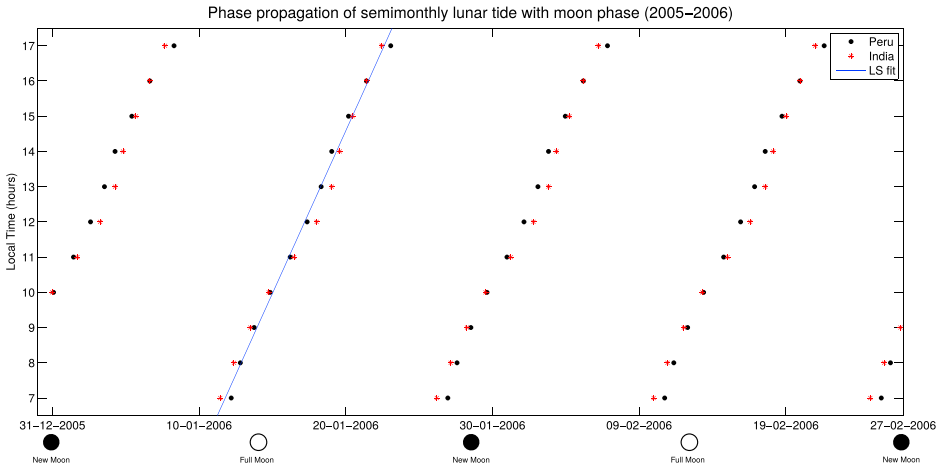

Figure 8. Phase propagation of the semimonthly lunar tide in the EEJ determined from *H* component of ground-based magnetic field recordings is presented as a function of moon phase during the 2005–2006 SSW event. Dots mark for each local time hour of the moon phase when the tidal wave crest is observed. The black dots and red asterisks represent the phase at Peruvian and Indian sectors, respectively. The blue line is obtained from least squares fitting to the propagating semimonthly lunar phase in the Peruvian sector.

4.3.2. 2009 SSW Event

We also determine the phase propagation of the semimonthly lunar tide during the 2008–2009 SSW event and is shown in Figure 9. The black dots and red asterisks mark the phase propagation in the Peruvian and Indian sectors, respectively, as seen earlier in Figure 8. The blue line is obtained by a linear regression fit made for the semimonthly propagating phase in the Peruvian sector (black dots). The phase propagation follows the expected pattern to a large extent in the Peruvian sector, but it deviates a small amount in the Indian sector during the noon hours before returning again to the expected values during evening. It seems that the lunar tidal effects over the Peruvian sector are stronger during this SSW than over the Indian sector. As the 2009 SSW is one of the strongest SSW events recorded in recent history [e.g., *Manney et al.*, 2009] and registered a strong amount of tropospheric forcing [e.g., *Ayarzagüena et al.*, 2011], it is possible that the phase of the semimonthly lunar tide gets slightly affected due to changed propagation conditions. However, since the semimonthly lunar phase still follows the expected values closely it would not be unreasonable to believe that the results largely pertain to lunar effects.

The equation of the regression line obtained by least squares fitting is given by

$$\mathrm{LT} = 0.95(d - d_0) + 8.3\,\mathrm{h} \tag{8}$$

Here equation ((8)) again resembles equation ((6)) which was derived from climatological analysis, thus verifying our approach.

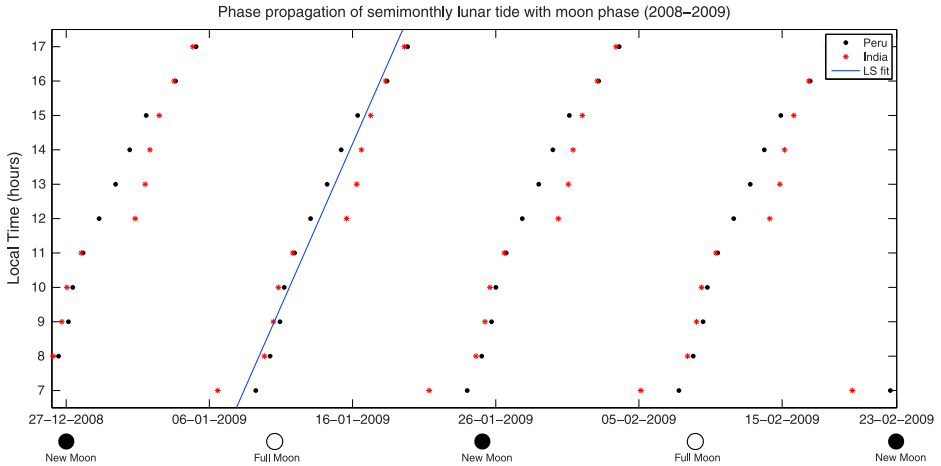

Figure 9. Same as Figure 8 except during 2008–2009 SSW winter.

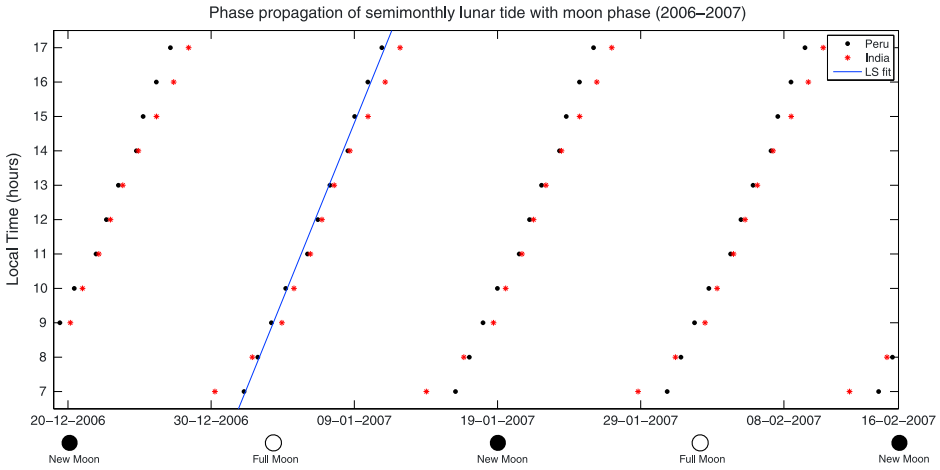

Figure 10. Same as Figure 8 except during 2006–2007 non-SSW winter.

4.3.3. 2006–2007 Northern Winter

Figure 10 presents the phase propagation of the semimonthly lunar tide at Peruvian and Indian sectors similar to Figure 8 except during the non-SSW winter of 2006–2007. A 59 day window is again selected starting from the day of new moon, and the phase propagation of the semimonthly lunar tide is determined as above. The pattern is again similar to the expected propagation in the Peruvian sector, whereas it diverges slightly in the morning hours in the Indian sector but returns back to the expected phase during later hours. The phase propagation in both the sectors closely resembles the climatology which leads us to believe that the results are largely related to lunar tide. We also obtained the equation of the regression line by least squares fitting as done previously

$$\mathrm{LT} = 1.0(d - d_0) + 8.1\ \mathrm{h} \tag{9}$$

and here also the regression parameters do not contradict the expected values from equation ((6)).

4.4. Climatological Analysis of Lunar Tidal Modulation of EEJ

We carry out a statistical study using the CHAMP peak EEJ intensity measurements to compare the climatological lunitidal amplitudes in EEJ over the Peruvian and Indian sector during December solstice.

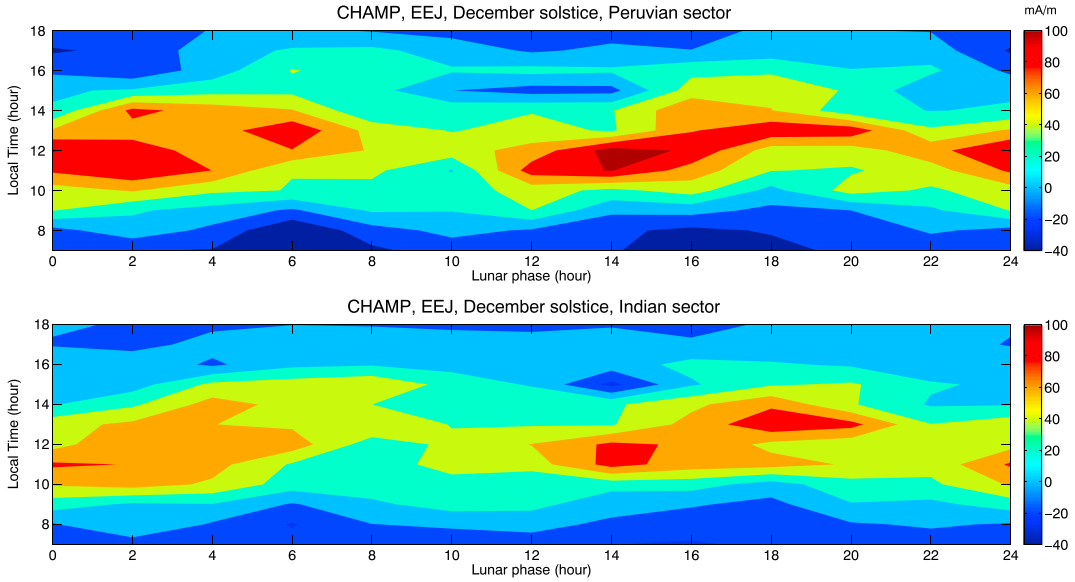

Figure 11. Local time variation of the electrojet lunar signal obtained using longitudinal averages of the EEJ peak current densities (mA/m) for the Peruvian and Indian sectors.

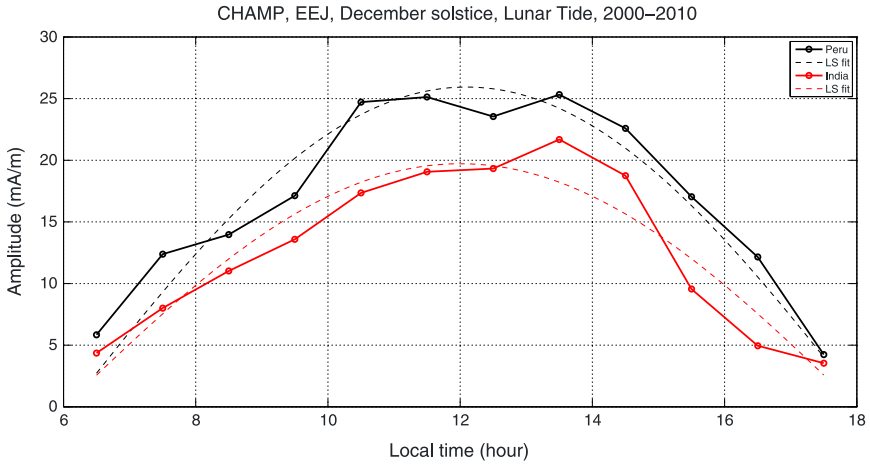

Figure 12. Comparison of the diurnal variation of the lunar tidal amplitude in the Peruvian (solid black line) and Indian (solid red line) sectors estimated using the CHAMP satellite data from 2000 to 2010 during December solstice. The dashed black and red lines represent the curves obtained after fitting (least squares) the square root of cosine to the climatological amplitudes in the Peruvian and Indian sectors, respectively.

In our analysis we use the entire peak EEJ measurements from 2000 to 2010 during December solstice (December to February). The procedure for sorting the data and further steps are explained as follows.

We consider the longitudinal intervals between 235°E–325°E and 45°E–135°E to represent the Peruvian and Indian sectors, respectively. The data are first sorted according to the longitudinal range of both the Peruvian and Indian sectors and then further sorted into bins of 2 h in moon phase and 1 h in local time (LT) for both the sectors. The local time interval here is again considered between 6 and 18 LT, as the EEJ signal outside of it is considered to be too weak. After sorting the data according to the moon phase and local time, there are on average 40 readings for each bin, from which a median value is calculated. Figure 11 shows the local time versus the moon phase distribution of the EEJ intensity obtained for both the Peruvian (top) and Indian (bottom) sectors. It is clear from the figure that the EEJ intensity in the Peruvian sector is larger than in the Indian sector. However, we are interested in quantitatively investigating the lunar signal in the EEJ in both plots, and a quantitative comparison is shown in Figure 12.

Since at a fixed local time, the lunar signal in the EEJ shows a semimonthly oscillation, we estimate the amplitude of this tide for local times between 6 and 18 LT. The local time dependence of this amplitude can be seen in Figure 12 for both the Peruvian (solid black line) and Indian (solid red line) sectors. From Figure 12 we can deduce that the lunar tidal amplitude of the EEJ over the Peruvian sector is larger than over the Indian sector for all local times between 6 and 18 LT. The diurnal variation of the semimonthly lunar tidal amplitude in both the sectors is also compared with the square root of cosine of the solar zenith angle which represents the electron density variation of a Chapman layer. The climatological lunitidal amplitudes in both the sectors are fitted with the function $\sqrt{A\cos(\mathrm{LT}-t_0)}$ using the least squares curve fitting method. The dashed black and the red lines represent the fitted curves in the Peruvian and Indian sectors, respectively. For the Peruvian sector the following values of A and t_0 were obtained: $A_{\mathrm{Peru}} = 25.94$ (mA/m) and $t_0 = 12.01$ h, and in case of the Indian sector the corresponding values were $A_{\mathrm{India}} = 19.71$ (mA/m) and $t_0 = 12.00$ h. From the curve fitting results, the ratio of peak amplitudes, $A_{\mathrm{Peru}}/A_{\mathrm{India}}$, equals 1.31 during the December solstice. These analyses suggest that climatological lunitidal amplitudes in EEJ are larger over the Peruvian sector than over the Indian sector.

5. Discussion

Our results clearly show the difference in lunitidal enhancements in EEJ and neutral temperature measurements during SSW and non-SSW periods in the Peruvian and Indian longitudinal sectors. Further, lunitidal enhancements in EEJ show a much greater longitudinal difference than in neutral measurements during SSWs.

Comparing our observations with the results obtained by *Sathishkumar and Sridharan* [2013], we find a good similarity. They estimated the M_2 amplitude in zonal wind at 90 km altitude at Tirunelveli for the 2009 SSW event, and their results showed a peak in M_2 amplitude on the day of peak PVW. They also determined

the M_2 amplitude in EEJ at Tirunelveli and found that its peak occurred approximately 2 weeks after the PVW, as seen in our results. Further, they also found that the enhancement in solar semidiurnal tide in EEJ was much larger than that in M_2 and concluded that the 2009 SSW event over Tirunelveli was mostly solar dominant. They performed the same analysis for the 2006 SSW event, but in this case their results showed that the M_2 amplitude in EEJ dominated over the solar semidiurnal tidal amplitude. Although we have not determined the solar tidal amplitudes in our study, we can discern from Figures 2 and 3 that the lunar influence during the 2006 SSW was strong over both the Peruvian and the Indian sectors, while during the 2009 SSW it was rather weak over the Indian sector. Based on this study we can state that while there can be a difference in lunar and solar tidal effects of the EEJ in different longitudinal sectors during the same SSW event, these effects can also be similar during another SSW event.

The connection between ionospheric variability and SSWs is generally accepted to be through the modulation of solar and lunar atmospheric tides [*Chau et al.*, 2012; *Pedatella et al.*, 2012; *Pedatella and Liu*, 2013]. Simulation results by *Pedatella and Liu* [2013] suggest that the ionospheric variability during major SSWs is primarily caused by the combined effects of the changes in migrating solar (SW2) and lunar semidiurnal (M_2) tides. The changes in the M_2 tide occur due to changes in tidal propagation conditions during SSWs which shift the Pekeris resonance peak closer to the M_2 period [*Forbes and Zhang*, 2012]. As the lunar tidal amplification is evident in SABER temperature measurements during the 2006 and 2009 SSW events, it may refer to the shift in Pekeris peak during both events. While there is a clear correlation between the lunitidal enhancements in the EEJ and in SABER temperature measurements during the 2006 SSW event in both the sectors, there is a lack of correlation between them in the Indian sector during the 2009 SSW event. From our observations and the results of *Sathishkumar and Sridharan* [2013] we can suggest that the semidiurnal enhancements during the 2009 SSW event over the Indian sector could be due to stronger modulation of EEJ by SW2 than by the M_2 tides. On the other hand, we find that the semidiurnal perturbations in EEJ over the Peruvian sector are strongly influenced by M_2 tides during both the 2006 and 2009 SSW events. It has also been suggested by *Pedatella and Liu* [2013] that planetary waves tend to damp the effects of SW2 tide in the Southern Hemisphere. There could also be a possibility that SW2 tidal effects at Huancayo are comparatively weaker than at Tirunelveli.

The M_2 amplitudes in neutral temperature measurements show lesser longitudinal variability during both the SSWs in the Peruvian and Indian sectors. Therefore, the longitudinal variability in the lunitidal enhancements in EEJ should be related to the electrodynamics in the *E* region dynamo. *Maute et al.* [2015] studied the longitudinal differences in $E \times B$ drift in the American and African sectors during the 2013 SSW event using the TIME-GCM simulations. The daytime vertical drift in the American sector showed an enhancement followed by progression of the daytime maximum from earlier to later local times, but in the African sector the daytime maximum vertical drift showed no local time progression. *Maute et al.* [2015] found that the penetrating electric fields during moderate geomagnetic activity could have partly caused the longitudinal difference in the daytime $E \times B$ in the two sectors. They conducted numerical experiments by shifting the neutral wind from the American sector to the African sector and vice-versa and found that the absence of semidiurnal shift to later hours in the African sector can be created due to the combination of neutral wind and the geomagnetic main field configuration. The 2009 and 2013 SSW event were both major warming events and similar in terms of strength of the polar vortex weakening. The semidiurnal perturbation in the EEJ in case of the 2009 SSW event is seen to be much stronger in the Peruvian/American sector but not so prominently in the Indian sector. This is similar to the observations of *Maute et al.* [2015] (see Figure 5) where the semidiurnal perturbation in $E \times B$ drift is weaker over the African sector during the 2013 SSW event. We therefore suggest that the findings of *Maute et al.* [2015] also provide one explanation for the longitudinal differences in the diurnal variation of the EEJ at Huancayo (Peru) and Tirunelveli (India) during the 2009 SSW event.

6. Conclusions

In this study we have computed the lunitidal amplitude during major SSW events of 2006 and 2009 and during the non-SSW winter of 2007 using (a) the *H* component recordings from Peruvian and Indian magnetic observatories, (b) the peak EEJ intensity data from CHAMP satellite, and (c) the SABER temperature measurements.

The evolution of derived tidal amplitudes from the three data sets is then compared during these periods in the Peruvian and Indian sectors. Major points of our study are as follows.

1. Our results show the difference in lunitidal enhancements in both the sectors during major SSWs and a non-SSW winter. It is observed that there is a significant lunitidal enhancement in all the three data sets during a major SSW event in comparison to a winter without an SSW.
2. Our results further show major longitudinal variabilities in lunitidal enhancements in EEJ in the Peruvian and Indian sectors. The semimonthly lunar tidal amplitude in EEJ shows similar enhancements in the Peruvian and Indian sectors during the 2006 major SSW event, but during the 2009 major SSW event lunar tidal enhancements in the Indian sector are much smaller and occur later with respect to the Peruvian sector.
3. The M_2 tidal amplitude derived from SABER temperature measurements is similar in both sectors and show a strong amplification during the 2006 and 2009 SSWs. The M_2 tidal amplitude during SSWs closely follows the semimonthly lunar tidal enhancements in the EEJ at Huancayo.
4. Our results suggest that the semimonthly lunar tidal enhancements in the EEJ are not uniform across all longitudes, and this could be either related to the local propagation conditions of the lunar tide or to the processes in the *E* region dynamo. Although, the 2006 and 2009 SSW events were similar with respect to their PVW strengths, the lunitidal enhancements are quite different.

Acknowledgments
The results presented in this paper rely on the data collected at Fuquene, Huancayo, Tirunelveli, and Alibag. We thank Instituto Geográfico Agustin Codazzi, Colombia, Instituto Geofisico del Peru, and Indian Institute of Geomagnetism for supporting geomagnetic observatory operations and INTERMAGNET for promoting high standards of magnetic observatory practice. We employ data from MERRA (Modern-Era Retrospective Analysis for Research and Applications). The data are downloaded from ftp://goldsmr3.sci.gsfc.nasa.gov/data/s4pa/MERRA/. The data for $F_{10.7}$ are obtained from the GSFC/SPDF OMNIWeb interface at http://omniweb.gsfc.nasa.gov. T.A.S. and C.S. thank the International Space Science Institute (ISSI) for providing support to the International Team on "A three-dimensional ground-to-space understanding of sudden stratospheric warmings." The discussions during these meetings were helpful in this study. Jürgen Matzka assisted in analyzing ground magnetometer data and global magnetic reference frames.

References

Alken, P., and S. Maus (2007), Spatio-temporal characterization of the equatorial electrojet from CHAMP, Ørsted, and SAC-C satellite magnetic measurements, *J. Geophys. Res.*, *112*, A09305, doi:10.1029/2007JA012524.

Andrews, D. G., J. R. Holton, and C. B. Leovy (1987), *Middle Atmosphere Dynamics*, vol. 40, Academic Press, New York.

Ayarzagüena, B., U. Langematz, and E. Serrano (2011), Tropospheric forcing of the stratosphere: A comparative study of the two different major stratospheric warmings in 2009 and 2010, *J. Geophys. Res.*, *116*, D18114, doi:10.1029/2010JD015023.

Bartels, A. J. (1936), Aufschlüsse über die Ionosphäre aus der Analyse sonnen-und mondentägiger erdmagnetischer Schwankungen, *Zeit. für Geophys.*, *12*, 368–378.

Bartels, J., and H. Johnston (1940), Geomagnetic tides in horizontal intensity at Huancayo, *Terr. Magn. Atmos. Electr.*, *45*(3), 269–308, doi:10.1029/TE045i003p00269.

Chau, J. L., B. G. Fejer, and L. P. Goncharenko (2009), Quiet variability of equatorial $E \times B$ drifts during a sudden stratospheric warming event, *Geophys. Res. Lett.*, *36*, L05101, doi:10.1029/2008GL036785.

Chau, J. L., N. A. Aponte, E. Cabassa, M. P. Sulzer, L. P. Goncharenko, and S. A. González (2010), Quiet time ionospheric variability over Arecibo during sudden stratospheric warming events, *J. Geophys. Res.*, *115*, A00G06, doi:10.1029/2010JA015378.

Chau, J. L., L. P. Goncharenko, B. G. Fejer, and H.-L. Liu (2012), Equatorial and low latitude ionospheric effects during sudden stratospheric warming events, *Space Sci. Rev.*, *168*(1–4), 385–417.

Chau, J. L., P. Hoffmann, N. M. Pedatella, V. Matthias, and G. Stober (2015), Upper mesospheric lunar tides over middle and high latitudes during sudden stratospheric warming events, *J. Geophys. Res. Space Physics*, *120*, 3084–3096, doi:10.1002/2015JA020998.

Cho, Y.-M., G. G. Shepherd, Y.-I. Won, S. Sargoytchev, S. Brown, and B. Solheim (2004), MLT cooling during stratospheric warming events, *Geophys. Res. Lett.*, *31*(10), L10104, doi:10.1029/2004GL019552.

Doumouya, V., J. Vassal, Y. Cohen, O. Fambitakoye, and M. Menvielle (1998), Equatorial electrojet at African longitudes: First results from magnetic measurements, *Ann. Geophys.*, *16*, 658–676.

Fang, T.-W., T. Fuller-Rowell, R. Akmaev, F. Wu, H. Wang, and D. Anderson (2012), Longitudinal variation of ionospheric vertical drifts during the 2009 sudden stratospheric warming, *J. Geophys. Res.*, *117*, A03324, doi:10.1029/2011JA017348.

Fejer, B. G., M. E. Olson, J. L. Chau, C. Stolle, H. Lühr, L. P. Goncharenko, K. Yumoto, and T. Nagatsuma (2010), Lunar-dependent equatorial ionospheric electrodynamic effects during sudden stratospheric warmings, *J. Geophys. Res.*, *115*, A00G03, doi:10.1029/2010JA015273.

Forbes, J. M. (1981), The equatorial electrojet, *Rev. Geophys.*, *19*(3), 469–504, doi:10.1029/RG019i003p00469.

Forbes, J. M., and X. Zhang (2012), Lunar tide amplification during the January 2009 stratosphere warming event: Observations and theory, *J. Geophys. Res.*, *117*, A12312, doi:10.1029/2012JA017963.

Forbush, S. E., and M. Casaverde (1961), *Equatorial Electrojet in Peru*, vol. 620, Carnegie Inst. of Washington, D. C.

Funke, B., M. López-Puertas, D. Bermejo-Pantaleón, M. García-Comas, G. P. Stiller, T. von Clarmann, M. Kiefer, and A. Linden (2010), Evidence for dynamical coupling from the lower atmosphere to the thermosphere during a major stratospheric warming, *Geophys. Res. Lett.*, *37*, L13803, doi:10.1029/2010GL043619.

Goncharenko, L., and S.-R. Zhang (2008), Ionospheric signatures of sudden stratospheric warming: Ion temperature at middle latitude, *Geophys. Res. Lett.*, *35*(21), L21103, doi:10.1029/2008GL035684.

Goncharenko, L. P., A. J. Coster, J. L. Chau, and C. E. Valladares (2010), Impact of sudden stratospheric warmings on equatorial ionization anomaly, *J. Geophys. Res.*, *115*, A00G07, doi:10.1029/2010JA015400.

Jadhav, G., M. Rajaram, and R. Rajaram (2002), A detailed study of equatorial electrojet phenomenon using Ørsted satellite observations, *J. Geophys. Res.*, *107*, SIA 12-1–SIA 12-12, doi:10.1029/2001JA000183.

Labitzke, K. (1972), Temperature changes in the mesosphere and stratosphere connected with circulation changes in winter, *J. Atmos. Sci.*, *29*(4), 756–766, doi:10.1175/1520-0469(1972)029<0756:TCITMA>2.0.CO;2.

Liu, H.-L., and R. G. Roble (2002), A study of a self-generated stratospheric sudden warming and its mesospheric–lower–thermospheric impacts using the coupled TIME-GCM/CCM3, *J. Geophys. Res.*, *107*(D23), 4695, doi:10.1029/2001JD001533.

Lühr, H., S. Maus, and M. Rother (2004), Noon-time equatorial electrojet: Its spatial features as determined by the CHAMP satellite, *J. Geophys. Res.*, *109*, A01306, doi:10.1029/2002JA009656.

Lühr, H., M. Rother, K. Häusler, P. Alken, and S. Maus (2008), The influence of nonmigrating tides on the longitudinal variation of the equatorial electrojet, *J. Geophys. Res.*, *113*, A08313, doi:10.1029/2008JA013064.

Lühr, H., T. A. Siddiqui, and S. Maus (2012), Global characteristics of the lunar tidal modulation of the equatorial electrojet derived from CHAMP observations, *Ann. Geophys.*, *30*(3), 527–536, doi:10.5194/angeo-30-527-2012.

Manney, G. L., M. J. Schwartz, K. Krüger, M. L. Santee, S. Pawson, J. N. Lee, W. H. Daffer, and R. A. Fuller (2009), Aura microwave limb sounder observations of dynamics and transport during the record-breaking 2009 Arctic stratospheric major warming, *Geophys. Res. Lett.*, *36*, L12815, doi:10.1029/2009GL038586.

Manoj, C., H. Lühr, S. Maus, and N. Nagarajan (2006), Evidence for short spatial correlation lengths of the noontime equatorial electrojet inferred from a comparison of satellite and ground magnetic data, *J. Geophys. Res.*, *111*, A11312, doi:10.1029/2006JA011855.

Matsuno, T. (1971), A dynamical model of the stratospheric sudden warming, *J. Atmos. Sci.*, *28*(8), 1479–1494.

Maute, A., M. E. Hagan, V. Yudin, H.-L. Liu, and E. Yizengaw (2015), Causes of the longitudinal differences in the equatorial vertical $E \times B$ drift during the 2013 SSW period as simulated by the TIME-GCM, *J. Geophys. Res. Space Physics*, *120*(6), 5117–5136, doi:10.1002/2015JA021126.

Onwumechilli, A. (1963), Lunar effect on the diurnal variation of the geomagnetic horizontal field near the magnetic equator, *J. Atmos. Terr. Phys.*, *25*(2), 55–70, doi:10.1016/0021-9169(63)90115-6.

Onwumechilli, C., and N. Alexander (1959), Variations in the geomagnetic field at Ibadan, Nigeria''–ii lunar and luni-solar variations in H and Z, *J. Atmos. Terr. Phys.*, *16*(1), 115–123, doi:10.1016/0021-9169(59)90014-5.

Park, J., H. Lühr, M. Kunze, B. G. Fejer, and K. W. Min (2012), Effect of sudden stratospheric warming on lunar tidal modulation of the equatorial electrojet, *J. Geophys. Res.*, *117*(A3), doi:10.1029/2011JA017351.

Pedatella, N. M., and H. Liu (2013), The influence of atmospheric tide and planetary wave variability during sudden stratosphere warmings on the low latitude ionosphere, *J. Geophys. Res. Space Physics*, *118*, 5333–5347, doi:10.1002/jgra.50492.

Pedatella, N. M., H.-L. Liu, A. D. Richmond, A. Maute, and T.-W. Fang (2012), Simulations of solar and lunar tidal variability in the mesosphere and lower thermosphere during sudden stratosphere warmings and their influence on the low-latitude ionosphere, *J. Geophys. Res.*, *117*, A08326, doi:10.1029/2012JA017858.

Rao, K. S. R., and K. R. Sivaraman (1958), Lunar geomagnetic tides at Kodaikanal, *J. Geophys. Res.*, *63*(4), 727–730, doi:10.1029/JZ063i004p00727.

Rastogi, R. (1962a), Enhancement of the lunar tide in the noon critical frequency of the f_2 layer over the magnetic equator, *J. Res. Nat. Bur. Stand.*, *66*, 601–606.

Rastogi, R. (1962b), Longitudinal variation in the equatorial electrojet, *J. Atmos. Terr. Phys.*, *24*(12), 1031–1040, doi:10.1016/0021-9169(62)90158-7.

Rastogi, R., and N. Trivedi (1970), Luni-solar tides in H at stations within the equatorial electrojet, *Planet. Space Sci.*, *18*(3), 367–377, doi:10.1016/0032-0633(70)90174-1.

Rastogi, R. G. (1963), Lunar tidal variations in the equatorial electrojet current, *J. Geophys. Res.*, *68*(9), 2445–2451, doi:10.1029/JZ068i009p02445.

Rigoti, A., F. H. Chamalaun, N. B. Trivedi, and A. L. Padilha (1999), Characteristics of the equatorial electrojet determined from an array of magnetometers in N-NE Brazil, *Earth Planets and Space*, *51*(2), 115–128, doi:10.1186/BF03352216.

Sathishkumar, S., and S. Sridharan (2013), Lunar and solar tidal variabilities in mesospheric winds and EEJ strength over Tirunelveli (8.7°N, 77.8°E) during the 2009 major stratospheric warming, *J. Geophys. Res. Space Physics*, *118*(1), 533–541, doi:10.1029/2012JA018236.

Scherhag, R. (1952), Die explosionsartigen stratosphärenerwärmungen des spätwinters 1951/52, *Ber. des Dtsch. Wetterdienstes in der US-Zone*, *6*(38), 51–63.

Siddiqui, T. A., H. Lühr, C. Stolle, and J. Park (2015a), Relation between stratospheric sudden warming and the lunar effect on the equatorial electrojet based on Huancayo recordings, *Ann. Geophys.*, *33*(2), 235–243, doi:10.5194/angeo-33-235-2015.

Siddiqui, T. A., C. Stolle, H. Lühr, and J. Matzka (2015b), On the relationship between weakening of the northern polar vortex and the lunar tidal amplification in the equatorial electrojet, *J. Geophys. Res. Space Physics*, *120*(11), 10,006–10,019, doi:10.1002/2015JA021683.

Stening, R. J., C. Carmody, and J. Du (2002), Simulating the lunar geomagnetic variations, *J. Geophys. Res.*, *107*, 12–11, doi:10.1029/2001JA000240.

Yamazaki, Y. (2013), Large lunar tidal effects in the equatorial electrojet during northern winter and its relation to stratospheric sudden warming events, *J. Geophys. Res. Space Physics*, *118*, 7268–7271, doi:10.1002/2013JA019215.

Yamazaki, Y., A. Richmond, and K. Yumoto (2012), Stratospheric warmings and the geomagnetic lunar tide: 1958–2007, *J. Geophys. Res.*, *117*, A04301, doi:10.1029/2012JA017514.

Zhang, X., and J. M. Forbes (2014), Lunar tide in the thermosphere and weakening of the northern polar vortex, *Geophys. Res. Lett.*, *41*(23), 8201–8207, doi:10.1002/2014GL062103.